Check for updates

The Meteoritical Society

Meteoritics & Planetary Science 56, Nr 7, 1293–1310 (2021)
doi: 10.1111/maps.13710

Exposure history, petrology, and shock-induced sulfidization reaction of Alatage Mountain 001 strewn field samples

Shijie LI [1,2]*, Ingo LEYA [3], Shijie WANG[4], Thomas SMITH [3,5], Huiming BAO[6,7], Yan FAN[1,8], and Bing MO[1,2]

[1]Center for Lunar and Planetary Sciences, Institute of Geochemistry, Chinese Academy of Sciences, Guiyang 550081, China
[2]Chinese Academy of Sciences Center for Excellence in Comparative Planetology, Hefei, China
[3]Physikalisches Institut, Universität Bern, Bern 3012, Switzerland
[4]State Key Laboratory of Environmental Geochemistry, Institute of Geochemistry, Chinese Academy of Sciences, Guiyang 550081, China
[5]State Key Laboratory of Lithospheric Evolution, Institute of Geology and Geophysics, Chinese Academy of Sciences, Beijing 100029, China
[6]Department of Geology and Geophysics, E235 Howe-Russell Geoscience Complex, Louisiana State University, Baton Rouge, Louisiana 70803, USA
[7]International Center for Isotope Effects Research and School of Earth Sciences and Engineering, Nanjing University, Nanjing 210023, China
[8]Department of Geology, Northwest University, Xi'an 710069, China
*Corresponding author. E-mail: lishijielpsc@mail.gyig.ac.cn; ldlshijie@126.com

(Received 03 March 2021; revision accepted 04 June 2021)

Abstract–Several hundred meteorites with a total mass of over 100 kg were collected as the Alatage Mountain (AM) strewn field located in the Kumtag desert, Xinjiang Province, China. Twelve AM meteorites were studied in this work. Petrography, mineralogy, bulk chemistry, bulk oxygen isotopic compositions, and light noble gas concentrations and isotopic compositions were determined for all or for a selection of the meteorites. The studied meteorites are L-chondrites that suffered a very strong impact; impact melt veins and melt pockets are widely distributed. More than 50% of the troilite exists in the form of blebs and veins in olivine and pyroxene. Some of these meteorites are impact melt recrystallized rocks (e.g., AM 037). The strong impact caused the decomposition of troilite, which led in AM 034 to the sulfidization reaction of olivine. The metal in most meteorites is almost completely altered, and the troilite has been significantly oxidized. Weathering resulted in the depletion of Mg, Fe, Co, and Ni, and the enrichment of Sr, Ba, Pb, and U in these meteorites. The cosmic ray exposure (CRE) ages measured for these specimens range between 6.2 ± 1.9 Ma and 9.0 ± 2.7 Ma, depending on the cosmogenic nuclide used. The average CRE age is 7.6 ± 1.3 Ma. Both ^{4}He and ^{40}Ar gas retention ages indicate that the strong impact which caused the shock effects occurred about 320 Ma ago.

INTRODUCTION

In the past 10 years (2012–2021), an increasing number of meteorites have been collected in the Gobi Desert, northwest of China. Some of those so-called dense collection areas (e.g., Alaer, Hami, Kumtag, Alatage Mountain [AM], Xingdi Argan, Loulan Yizhi, Lop Nur, Tuya, Lenghu, Tuanjie) have been presented in recent publications (Li and Hsu 2014; Li et al. 2017a; Zeng et al. 2018; Du et al. 2021; Meteoritical Bulletin Database [MBD]). However, many of the meteorites found in any single area may be part of a strewn field. Three strewn fields (Tuya 002-007, Kumtag 016, and Kumtag) in the Tuya and Kumtag dense areas have already been identified (Li et al. 2017a; Zeng et al. 2018; Du et al. 2021). In 2013, we formed a meteorite research team and collected 42 meteorites in a 1 × 3 km area on the eastern flank of AM in the Kumtag desert, Xinjiang, China

© 2021 The Meteoritical Society (MET)

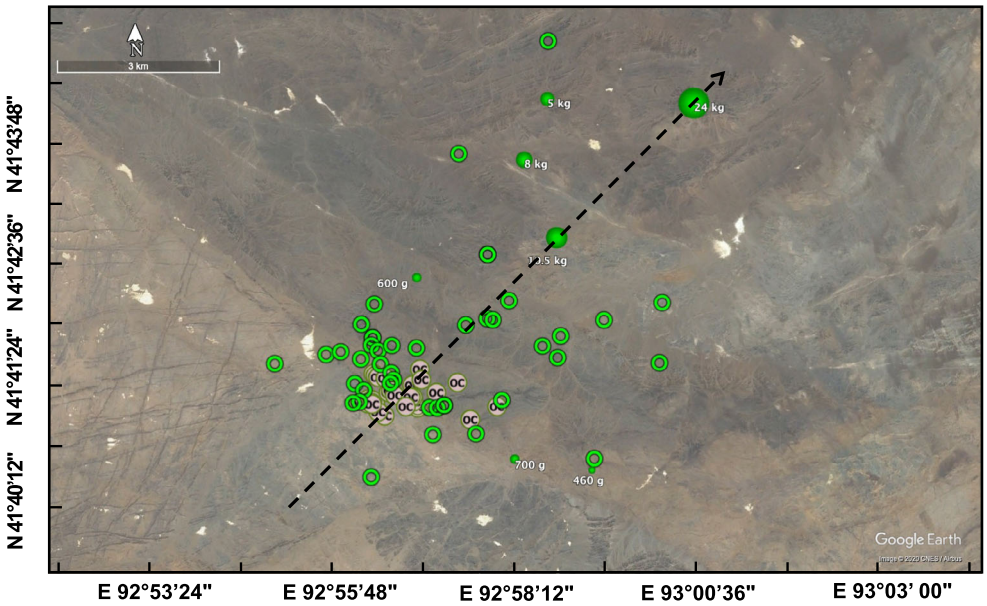

Fig. 1. Distribution of meteorites from the AM meteorite strewn field. The length of the strewn field is only two times the width, indicating a relatively high entry angle of the meteoroid. Open green circles represent the meteorites with unknown masses. Solid green symbols represent the meteorites with known masses. Solid brown symbols marked with OC represent the meteorites whose names have been approved by the Meteoritical Society as official names. The dotted arrow indicates the possible landing direction of the AM meteoroid. The base map is from Google Earth. (Color figure can be viewed at wileyonlinelibrary.com.)

(Fig. 1). Later, these 42 meteorites were named AM 001–042 (MBD), whereas this paper will refer to the strewn field as AM 001. In 2015, a meteorite hunter team collected several large meteorites about 4–8 km northeast of the location searched by us in 2013. Four meteorites with masses greater than 5 kg have been recovered; the largest mass is about 24 kg. With the find locations kindly provided by the other meteorite hunters, a meteorite strewn field with an SW–NE orientation was identified (Fig. 1). This strewn field is located only 12 km west of the Kumtag meteorite strewn field (Du et al. 2021). Considering the still incomplete statistics, the total mass of the hundreds of specimens collected in this strewn field is probably greater than 100 kg. The length and the width of the strewn field are about 5 and 10 km, respectively, indicating a relatively high angle of entry of this meteoroid.

In this study, we selected 12 samples (Table 1) collected in the AM area for a study of their mineralogy, petrology, bulk chemistry, and cosmic ray exposure (CRE) history. Among these samples, the two meteorites AM 029 and AM 037 were selected for whole rock oxygen isotopic analysis.

SAMPLES AND METHODS

Petrographic investigations were carried out at the Institute of Geochemistry, Chinese Academy of Sciences, with a Scios-FIB field emission scanning electron microscope (SEM) equipped with an EDAX energy dispersive X-ray spectrometer (EDS). For each of the 12 selected samples, we prepared polished sections for petrographic investigations and mineral chemical composition analysis (Table 1).

Noble gas measurements were carried out at the University of Bern, Switzerland, on two self-made noble gas mass spectrometers. The measurement method, the data reduction, the calculation of the CRE age, and the gas retention age follow the same procedures and methods as previously reported in Li et al. (2017b) and Zeng et al. (2018). Electron probe microanalysis (EPMA) was performed at the Guilin University of Technology. The analysis standards we used and the test conditions were the same as in Zeng et al. (2018). The standard ZAF correction procedure was used for data calculation.

The bulk oxygen isotopic compositions of AM 029 and AM 037 were measured at Louisiana State University (LSU) using the same method as reported in Li et al. (2011, 2018). The Jilin meteorite (H5) was selected as a reference material and was measured together with two AM meteorites.

The major and trace element analyses were performed at the Guizhou Tongwei Analytical Technology Co. Ltd. For trace element measurement, approximately 50 mg of each meteorite powder was dissolved in a Teflon bomb with a double distilled concentrated HNO_3-HF (1:4) mixture. The bomb and

Table 1. EPMA analysis giving the average composition (wt%) of representative olivine, low-Ca pyroxene, and plagioclase in AM meteorites.

					Low-Ca pyroxene (mole%)		Plagioclase (mole%)					
Name	Mass	Type	Shock	Weathering	Fa (mole%)	Fs	Wo	An	Or	Oxygen isotope	Bulk chemistry	Noble gas
AM 004	12.2	L5	S5	W3	25.0 ± 0.5	20.7 ± 0.3	1.8 ± 0.2	22.1 ± 2.9	2.5 ± 0.8	–	–	–
AM 006	17.4	L5	S5	W3	24.6 ± 0.4	20.8 ± 0.2	1.9 ± 1.0	–	–	–	√	√
AM 014	18.3	L5	S5	W3	24.3 ± 0.3	20.2 ± 0.3	1.5 ± 0.3	–	–	–	√	√
AM 021	37.8	L5	S5	W3	24.9 ± 0.6	21.4 ± 0.6	1.5 ± 0.2	12.0 ± 2.1	5.9 ± 1.3	–	√	√
AM 024	240	L5	S5	W3	25.1 ± 0.4	21.4 ± 0.4	1.4 ± 0.1	11.1 ± 1.8	5.4 ± 0.9	–	–	√
AM 029	44.7	L5	S5	W3	25.1 ± 0.3	21.4 ± 0.3	1.5 ± 0.1	10.5 ± 0.4	4.0 ± 0.9	√	–	√
AM 033	23.1	L5	S5	W3	25.0 ± 0.3	21.3 ± 0.6	1.3 ± 0.1	10.8 ± 0.5	5.2 ± 0.7	–	√	√
AM 034	101.6	L5	S5	W3	25.2 ± 0.7	20.4 ± 0.3	1.8 ± 0.3	16.2 ± 7.1	3.9 ± 2.1	–	√	√
AM 036	24.8	L5	S5	W3	24.1 ± 0.4	21.0 ± 0.6	1.6 ± 0.3	14.1 ± 4.3	4.3 ± 1.1	–	–	√
AM 037	18.9	Melt breccia (MB)	<S2	W3	24.3 ± 0.6	20.7 ± 0.3	1.3 ± 0.3	4.0 ± 0.3	12.1 ± 2.1	√	√	√
AM039	67.6	L5	S5	W3	24.6 ± 0.3	21.0 ± 0.4	2.0 ± 0.5	–	–	–	√	√
AM040	97.2	L5	S5	W2	25.5 ± 0.3	21.4 ± 0.4	1.8 ± 0.2	21.5 ± 7.6	2.8 ± 1.6	–	√	√

its contents were maintained in an oven at 185 °C for 72 h. Sample residues after HF evaporation were redissolved with double distilled concentrated HNO_3. They were then dried, redissolved in 2N HNO_3, dried again, and taken up in 3 mL 2 N HNO_3 stock solution. Finally, the solution was diluted to 1/4000 with 2% HNO_3 together with the addition of 10 ppb ^{61}Ni, 6 ppb Rh, In, and Re internal spikes. Next, the samples were analyzed using a Thermal X series 2 inductively coupled plasma mass spectrometer (ICP-MS) equipped with a Cetac ASX-510 Autosampler.

For major element analysis, a separate weighed portion of each powdered sample (typically ~1 g) was dried in an oven at 105 °C for 8 h. The whole rock powder sample was placed in a ceramic crucible and ignited in a muffle furnace at 1000 °C for 200 min. Then, the sample was transferred to a drying dish when cooling down to approximately 200 °C. After the sample cooled down to room temperature, we weighed the sample and estimated the amount of material lost by ignition. The ignited sample (0.6 g) was evenly mixed with 6 g flux material (49.75% $Li_2B_4O_7$: 49.75% $LiBO_2$: 0.5% LiBr) in a ceramic crucible, then transferred into a platinum crucible, and was melted at 1100 °C for 7 min. Finally, the sample melt was poured into a mold and cooled to form a glass sheet, which was later measured on an AxiosMAX X-ray fluorescence (XRF).

RESULTS

Petrography and Mineral Chemistry

All meteorite specimens collected in this strewn field have similar features; they are gray-black in color, free of fusion crust, and exhibit rust on the surface that was in contact with the ground (Figs. 2a–g). Texturally, the 12 meteorites investigated can be divided into two different groups; recrystallized achondritic (AM 037) (Fig. 3) and heavily shocked (S5) chondritic (the other samples) (Figs. 4 and 5).

For AM 037, the lithology (Fig. 3a) exhibits a porphyritic texture, composed of ~5 vol% unmelted precursor chondritic clasts (Fig. 3b) and of ~10 vol% spherical to ellipsoid rust nodules (Figs. 3a and 3c) set in a matrix mainly composed of microphenocrysts of olivine, pyroxene, and feldspar glass (Figs. 3b–e). The unmelted clasts are 20–400 μm in size (mostly 100 μm) and usually contain abundant tiny troilite and Fe-Ni metal dots (Figs. 3a and 3b). Obviously, the rust nodules (50–1000 μm in size) are produced by terrestrial weathering of previously existing Fe-Ni metal and troilite nodules (Fig. 3a and 3c). The ellipsoid nodules tend to be oriented along their long axes (Fig. 3a). Olivine and pyroxene in the matrix are several microns

Fig. 2. Photos of some representative meteorites collected in the AM area. a–d) The surfaces of the meteorites collected within the AM strewn field are black and with no fusion crust, indicating a relatively long terrestrial age. d) Largest meteorite (~24 kg) collected in AM strewn field. e) The front of the meteorite is covered with a brown rusty layer, indicating that this surface was once in contact with the ground for a long time. f, g) Limonite disseminates in the ground-contacting surface of the meteorite, which is a typical characteristic of hot desert ordinary chondrites. (Color figure can be viewed at wileyonlinelibrary.com.)

to ~50 μm in size, with K-rich feldspar glass (<10 μm) and inhomogeneously distributed troilite plus Fe-Ni metal (<50 μm) as mesostasis (Figs. 3b–e). Pyroxene in troilite-rich areas tends to be euhedral crystals (Fig. 3d). Pyroxene in the matrix is generally larger in size than olivine and frequently contains olivine inclusions (Figs. 3d and 3e). Almost all phosphate minerals (apatite and merrillite) in this sample occur at the margin of spherical Fe-Ni metal and troilite nodules (Figs. 3c and 3e).

The meteorites of the second group (AM 004, AM 006, AM 014, AM 021, AM 024, AM 029, AM 033, AM 034, AM 036, AM 039, and AM 040) have a mineral assemblage typical for ordinary chondrites (i.e., olivine, low-Ca pyroxene, plagioclase, high-Ca pyroxene, Fe-Ni metal, troilite, and some minor minerals). Various types of chondrules with different sizes (200–3000 μm) have been observed in the samples (e.g., Fig. 4). Although most of the chondrule boundaries are not clear, for the majority of the chondrules, the structures are distinguishable (e.g., Fig. 4). The most significant characteristics of these meteorites are ~50 vol% of troilite present as veins and dots mainly in olivine and pyroxene and relatively less in apatite, chromite, and plagioclase (from <1 μm to several microns) (Figs. 5a and 5b). Almost all Fe-Ni metal and parts of the troilite in the studied polished sections are heavily altered due to terrestrial weathering, which filled the fractures in various widths (Figs. 5a–c). Plagioclase shows various irregular borders and occupies interstitial space between other minerals or cracks within olivine and pyroxene (Fig. 5). Acicular apatite druses were observed in the studied sections of AM 034 and AM 039 (Fig. 5d). A type of unique melt vein and pocket occurs in these samples (Figs. 5e and 5f). The melt veins and pockets are composed of feathery feldspar glass, low-Ca, high-Ca pyroxene, ±olivine, troilite, and Fe-Ni metal (Figs. 5e and 5f). Large minerals in melt veins and pockets are almost free of fracture, Fe-Ni, and troilite dots (Figs. 5e and 5f). One melt pocket in a merrillite grain, composed of feldspar glass, merrillite, troilite, and Fe-Ni metal, was observed in AM 040 (Fig. 5g). In a melt pocket, small high-Ca pyroxene grains (1–2 μm) scatter in relatively coarse feathery feldspar glass (Fig. 5h). In the studied thick section of AM 034, a troilite–pyroxene (low-Ca)–olivine intergrowth (TPOI) in an olivine grain was observed (Fig. 6). Some low-Ca pyroxene in TPOI

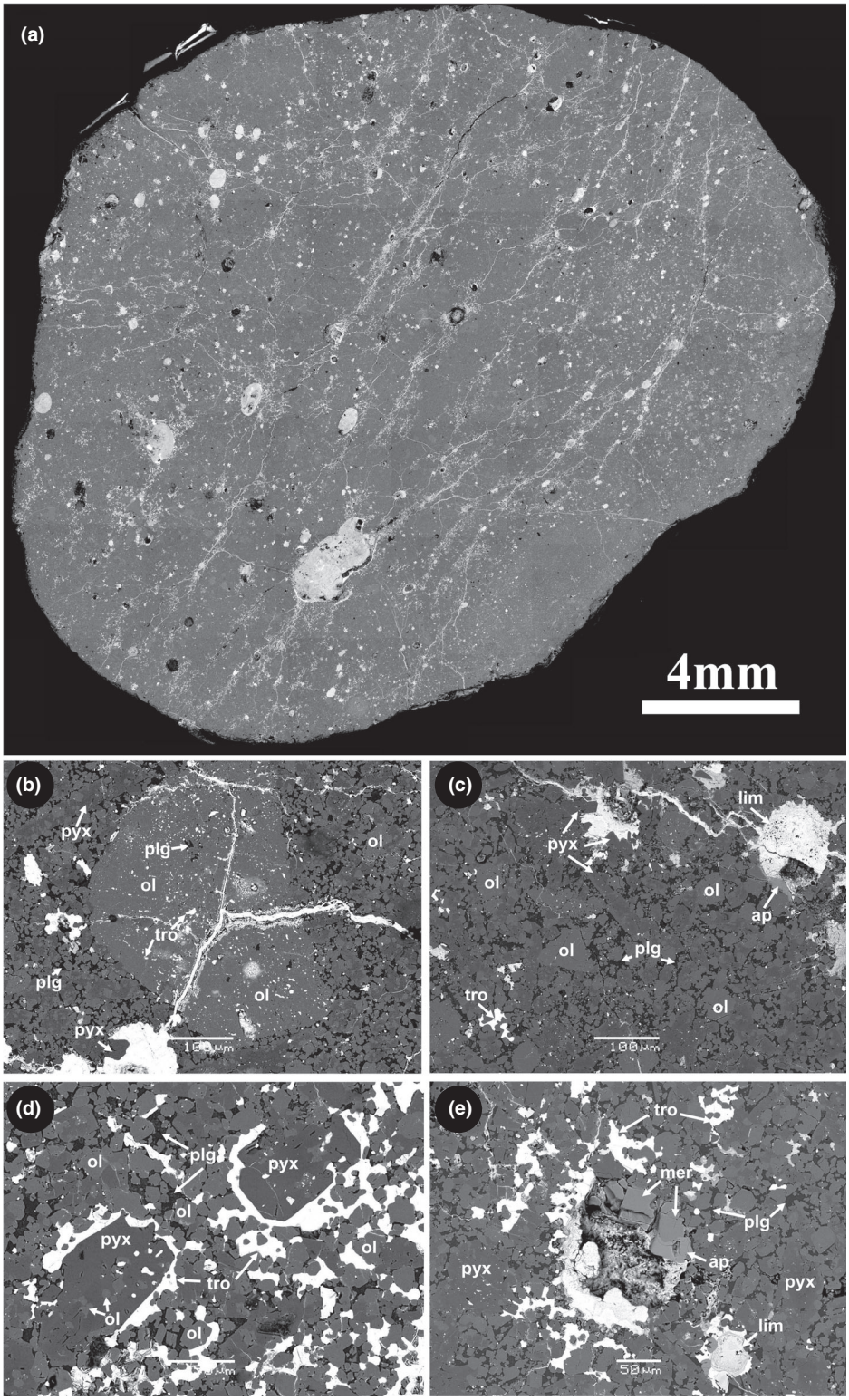

Fig. 3. The BSE images of AM 037. a) The polished section showing an achondritic structure. All original Fe-Ni metal and troilite have been altered by terrestrial weathering and occur as spherical to ellipsoidal nodules. b) Unmelted clast in the polished section, which is too small to be seen in (a). c) The matrix of the meteorite. d) Euhedral pyroxene crystals in a troilite-rich area. e) Phosphate commonly occurs next to Fe-Ni metal (altered) nodules. Ol = olivine; pyx = pyroxene; lim = limonite; plg = plagioclase; tro = troilite; mer = merrillite; ap = apatite.

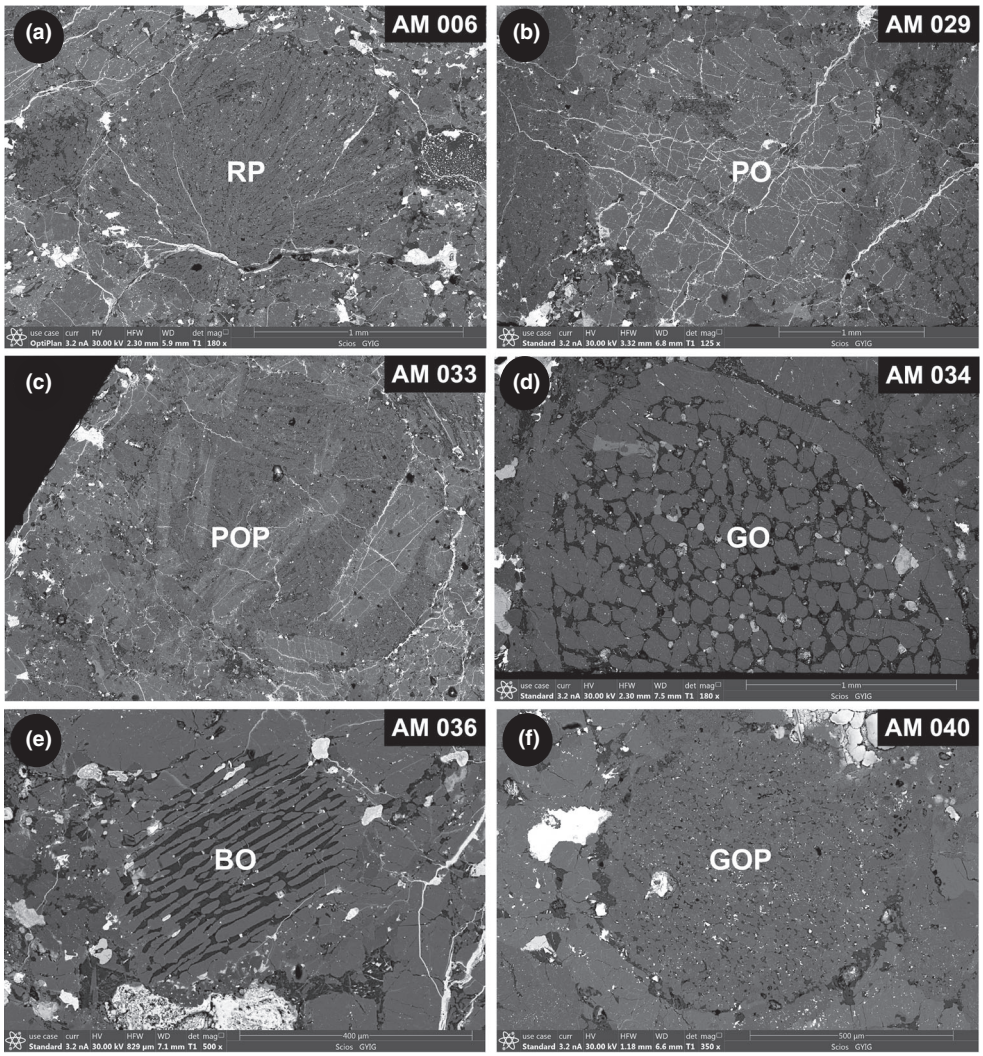

Fig. 4. BSE images of chondrules in AM meteorites. a) A radial pyroxene (RP) chondrule in AM 006. b) A porphyritic olivine (PO) chondrule in AM 029. c) A porphyritic olivine pyroxene (POP) chondrule in AM 033. d) A granular olivine (GO) chondrule with an olivine rim in AM 034. e) A barred olivine (BO) chondrule in AM 036. f) A granular olivine pyroxene (GOP) chondrule in AM 040. Except for the GO in (d), the boundaries of the other chondrules are indistinguishable from the surrounding minerals.

shows the deficiency of Fe and Ca compared to the rest of other low-Ca pyroxenes in AM 034.

The composition of representative olivine, low-Ca pyroxene, and plagioclase (or feldspar glass) of the studied meteorites is given in Table 1; detailed EPMA analysis data are given in Table S1 in supporting information. Fe and Mg contents of olivine and low-Ca pyroxene are in a very narrow range. AM 004 and AM 036 have the highest and lowest average Fa values (25.0 ± 0.5 mole% and 24.1 ± 0.4 mole%), respectively. AM 014 and AM 021 have the highest and lowest average Fs values (20.2 ± 0.3 mole% and 21.4 ± 0.6 mole%), respectively. However, the composition of plagioclase is much more variable even within one sample. The average An and Or values of feldspar glass in AM 037 are 4.0 ± 0.3 mole% and 12.1 ± 2.1 mole%, respectively. The corresponding values of other studied samples varied between 10.5 ± 0.4–22.1 ± 2.9 mole% and 2.5 ± 0.8–5.9 ± 1.3 mole%, respectively. Clearly, the K content of feldspar glass in AM 037 is significantly higher than that in the plagioclase of other samples. Some pyroxene grains located in TPOI in AM 034 show Fe and Ca deficits when compared to the composition of low-Ca pyroxene in other parts of AM 034 as well as in other studied samples (Figs. 6 and 7). The EPMA analysis data of olivine and pyroxene in TPOI in MA 034 are reported in Table S2 in supporting information.

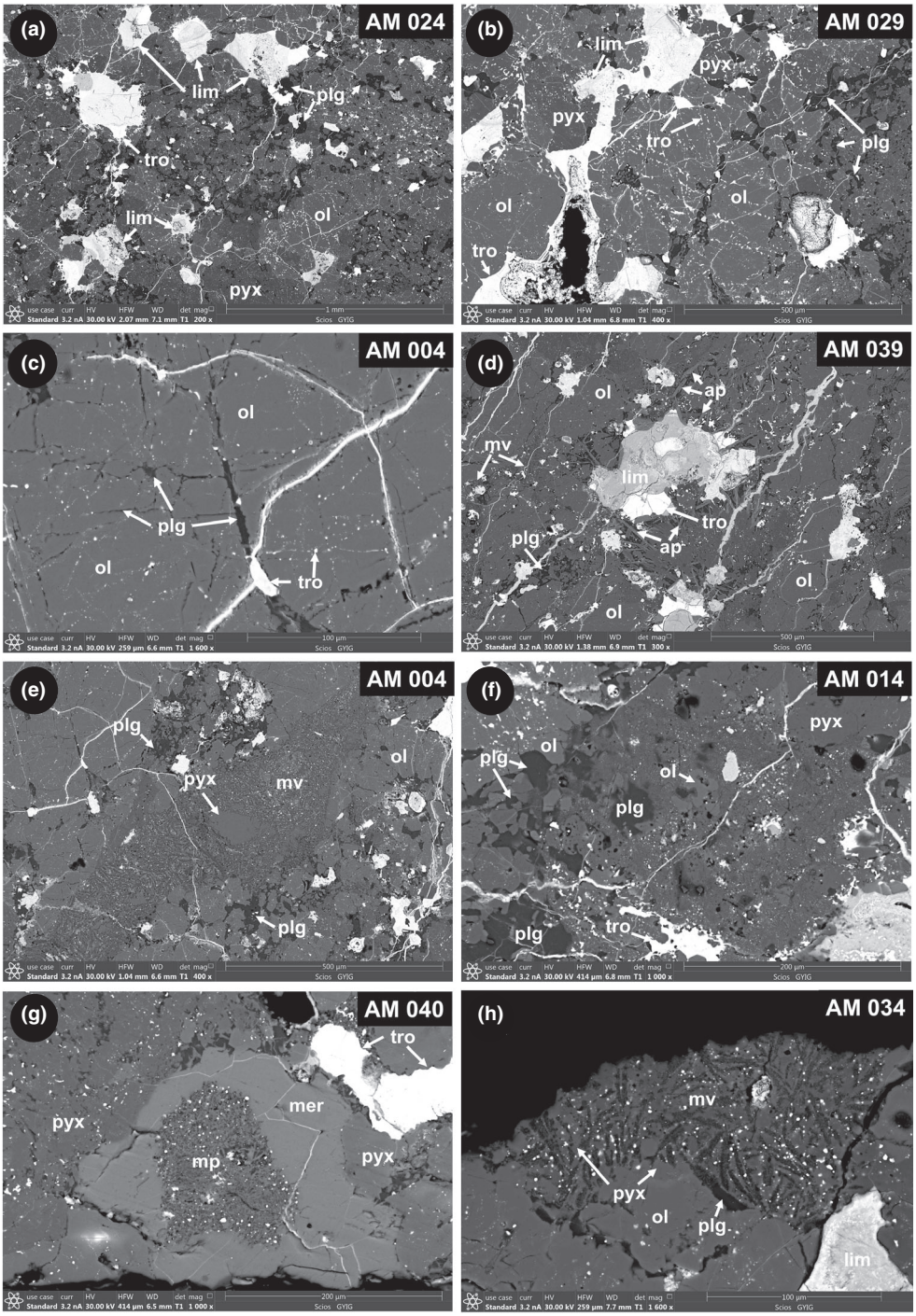

Fig. 5. BSE images of AM chondrites. a, b) About half of the troilite exists as veins and blebs in most of the olivine and pyroxene grains (e.g., in AM 024 and AM 029, respectively). c) Plagioclase in AM 004 occurs as veins in an olivine grain. d) Acicular apatite druses next to Fe-Ni metal (mainly altered as weathering products). e) A unique shock melt vein (mv) in AM 004. This kind of mv is common in AM chondrites. The mv is mainly composed of pyroxene, feathery feldspar glass, troilite, and other minor components. f) Shock melt pocket (mp) in AM 014. g) The mp in an apatite grain in AM 040. h) A relatively coarse mv in AM 034. The mv is mainly composed of feathery feldspar glass with very small high-Ca pyroxene inclusions and low-Ca pyroxene. The white dots are troilite and Fe-Ni metal.

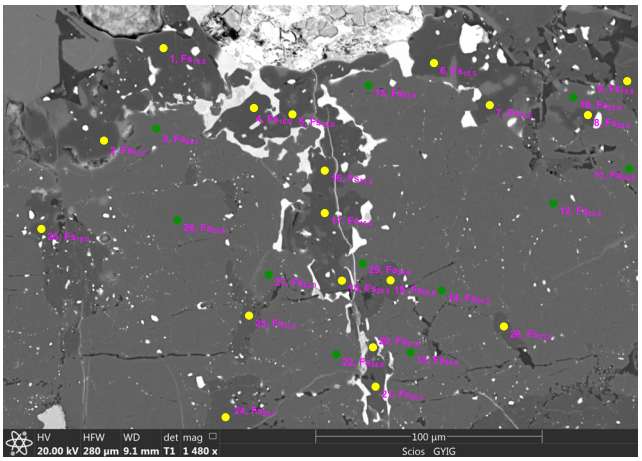

Fig. 6. BSE image of a troilite–pyroxene (low-Ca)–olivine intergrowth (TPOI) in AM 034. The TPOI is mainly composed of olivine, low-Ca pyroxene, and troilite. Some low-Ca pyroxene is Fe and Ca poor compared to that in other locations in AM 034 and other AM meteorites. (Color figure can be viewed at wileyonlinelibrary.com.)

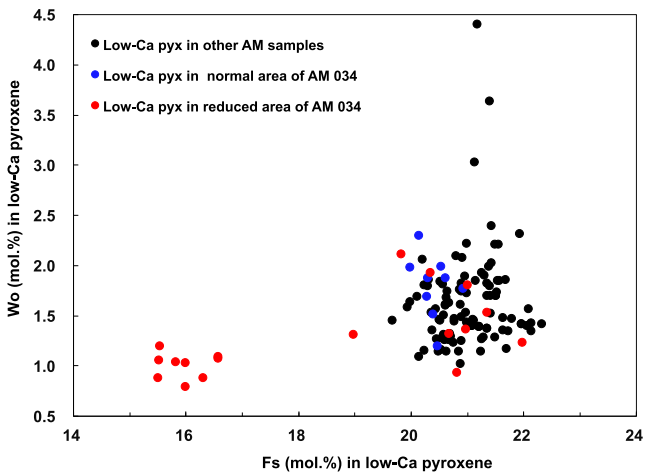

Fig. 7. Low-Ca pyroxene ferrosilite (Fs) versus wollastonite (Wo) contents of AM meteorites and TPOI in AM 034. (Color figure can be viewed at wileyonlinelibrary.com.)

Bulk Chemistry

The whole rock major and trace element contents measured in eight AM samples are given in Table 2. The composition of olivine and low-Ca pyroxene indicates these meteorites are ordinary chondrites (Table 1). Therefore, we normalized the bulk chemistry data of these samples to the corresponding data for L chondrites reported by Lodders and Fegley (1998) (Fig. 8). Mg, Fe, Co, and Ni contents are ~20% lower than those of ordinary L chondrites, while Sr, Ba, Pb, and U are significantly higher than those of L chondrites. Pb in AM 006 and AM 037 is more than 10 times higher than the average L content. Except for AM 021 and AM 039, U contents are more than 10 times higher than L chondrite averages. Rare earth elements (REEs) in AM 006 are slightly higher than in the average L chondrite composition. AM 006, AM 014, and AM 037 show slight LREE enrichments (Fig. 8).

Oxygen Isotopic Composition

Two aliquots of each AM 029 and AM 037 were analyzed; the results are given in Table 3. The average values of $\delta^{18}O$, $\delta^{17}O$, and $\Delta^{17}O$ of the two AM 029 aliquots are $5.15 \pm 0.07‰$, $3.67 \pm 0.02‰$, and $0.96 \pm 0.02‰$, respectively. The corresponding values of two AM 037 aliquots are $4.40 \pm 0.28‰$, $3.20 \pm 0.15‰$, and $0.88 \pm 0.01‰$, respectively. The oxygen isotopic compositions of the two meteorites are in the range typical for L group ordinary chondrites (Fig. 9).

Light Noble Gas Analyses

The He, Ne, and Ar isotopic compositions of 11 meteorite specimens were measured. For each sample, the basic information together with the concentrations and isotopic ratios, corrected for blank and instrumental mass fractionation, are compiled in Table 4. The ^{3}He, ^{4}He, ^{20}Ne, ^{36}Ar, and ^{38}Ar contents (all in units of 10^{-8} cm^3 STP/g) are in the ranges of 10.08 ± 0.25–13.01 ± 0.36, 133.6 ± 3.7–183.2 ± 1.6, 2.94 ± 0.03–4.33 ± 0.32, 3.35 ± 0.06–10.23 ± 0.75, and 1298 ± 83–3408 ± 104, respectively. The ratios of $^{21}Ne/^{22}Ne$, $^{20}Ne/^{22}Ne$, and $^{36}Ar/^{38}Ar$ are between 0.891 ± 0.014–0.919 ± 0.014, 0.891 ± 0.014–1.239 ± 0.019, and 3.22 ± 0.06–4.55 ± 0.11, respectively. These ratios indicate that, in addition to cosmogenic noble gases, there is a trapped component, which will be discussed further below.

DISCUSSION

Petrology, Shock Degree, Weathering, and Classification

Except for AM 037, the investigated meteorites show characteristics of petrographic type 5 (Figs. 4 and 5). The Fa and Fs values of olivine and low-Ca pyroxene in these meteorites are in a very narrow range and are consistent with the typical values for L chondrites (Fig. 10). Fe-Ni metal almost completely oxidized into rust and also troilite is significantly altered, which indicates that these samples have been heavily weathered. Shock veins, shock pockets, melt veins of plagioclase, planar fractures (filled with troilite) in olivine, and pyroxene are all well developed in the studied meteorites (except AM 037). These features indicate a very strong impact event, which generated a

Table 2. Whole-rock chemical composition of eight AM meteorites.

Element	AM 006	AM 014	AM 021	AM 033	AM 034	AM 037	AM 039	AM 040	Method
Li (μg g^{-1})	1.75	1.68	1.60	1.44	1.67	2.04	1.59	1.78	ICP-MS
Na (μg g^{-1})	7311	6768	6897	6477	6596	6669	6571	7321	XRF
Mg (%)	12.6	12.7	13.1	12.0	13.2	13.3	11.8	13.3	XRF
Al (%)	1.17	1.10	1.13	1.09	1.08	1.16	1.08	1.17	XRF
Si (%)	21.5	20.9	21.4	21.0	21.4	18.1	21.8	21.6	XRF
P (μg g^{-1})	1240	1140	1260	1140	932	1100	1160	1100	ICP-MS
K (μg g^{-1})	930	818	804	656	778	855	777	857	XRF
Ca (%)	1.47	1.33	1.32	1.25	1.28	1.29	1.28	1.28	XRF
Sc (μg g^{-1})	8.70	8.24	8.57	7.9	8.31	7.74	7.90	8.42	ICP-MS
Ti (μg g^{-1})	709	707	642	691	725	600	652	689	XRF
V (μg g^{-1})	68.5	68.6	67.4	66.9	71.8	68.1	67.5	74.9	ICP-MS
Cr (μg g^{-1})	3960	4030	3910	4080	4160	4070	3890	4490	ICP-MS
Mn (μg g^{-1})	2520	2500	2540	2420	2620	2370	2420	2640	ICP-MS
Fe (%)	18.5	19.8	18.3	20.0	18.0	18.8	19.6	16.8	XRF
Co (μg g^{-1})	403	491	455	484	435	399	433	405	ICP-MS
Ni (%)	0.929	1.00	1.02	0.972	1.00	0.818	1.03	1.09	ICP-MS
Cu (μg g^{-1})	66.5	78.1	62.8	86.5	79.7	86.4	97.8	78.5	ICP-MS
Zn (μg g^{-1})	51.6	51.2	51.9	50.7	54.5	50.1	49.8	58	ICP-MS
Ga (μg g^{-1})	5.17	5.31	5.30	5.15	5.02	5.62	5.27	5.69	ICP-MS
Rb (μg g^{-1})	2.53	2.28	2.30	1.68	2.28	2.67	2.28	2.91	ICP-MS
Sr (μg g^{-1})	23.1	20.9	19.3	21.4	15.4	59.5	26.1	20.2	ICP-MS
Y (μg g^{-1})	2.48	2.23	2.19	2.09	2.05	1.99	2.10	2.22	ICP-MS
Zr (μg g^{-1})	5.99	5.84	5.98	5.43	5.52	5.70	5.51	5.98	ICP-MS
Nb (μg g^{-1})	0.412	0.484	0.386	0.467	0.419	0.411	0.419	0.437	ICP-MS
Ba (μg g^{-1})	15.3	15.4	11.9	10.5	7.53	35.5	8.76	21.7	ICP-MS
La (ng g^{-1})	493	420	358	340	297	413	335	384	ICP-MS
Ce (ng g^{-1})	1220	1050	916	883	779	1010	870	940	ICP-MS
Pr (ng g^{-1})	177	153	139	132	120	146	131	143	ICP-MS
Nd (ng g^{-1})	823	739	688	652	593	684	659	708	ICP-MS
Sm (ng g^{-1})	260	234	227	209	198	207	212	224	ICP-MS
Eu (ng g^{-1})	83.5	81.1	81.3	78.7	75.3	77.7	79.4	85.2	ICP-MS
Gd (ng g^{-1})	340	296	291	273	265	266	281	291	ICP-MS
Tb (ng g^{-1})	62.5	55.9	54.0	51.5	49.7	49.4	51.3	54.5	ICP-MS
Dy (ng g^{-1})	410	358	354	340	323	328	345	356	ICP-MS
Ho (ng g^{-1})	90.7	80.0	80.3	74.5	73.4	74.2	76.5	79.9	ICP-MS
Er (ng g^{-1})	264	237	232	217	218	211	224	236	ICP-MS
Tm (ng g^{-1})	41.3	37.3	36.6	34.6	35.0	33.8	36.0	37.8	ICP-MS
Yb (ng g^{-1})	266	241	239	227	223	219	231	241	ICP-MS
Lu (ng g^{-1})	40.9	37.9	37.4	35.9	36.3	35.3	36.1	37.9	ICP-MS
Hf (ng g^{-1})	165	160	162	144	149	155	152	166	ICP-MS
Ta (ng g^{-1})	20.4	25.2	19.4	23.5	19.4	21.0	20.5	21.0	ICP-MS
Pb (ng g^{-1})	1760	318	209	158	342	550	132	356	ICP-MS
Th (ng g^{-1})	54.8	77.1	55.1	54.6	46.7	93.3	50.3	61.8	ICP-MS
U (ng g^{-1})	205	190	121	199	185	347	128	254	ICP-MS
LOI (%)	0.59	0.32	0.50	1.14	1.12	2.82	0.40	2.12	

The uncertainties of Na, Mg, K, Ca, Fe, Co, and Ni are lower than 0.1%, the uncertainties of trace elements are ~10%.

pressure in the range of 75–90 GPa (defined as S6 in Stoffler et al. 1991). The absence of fractures, Fe-Ne metal, and troilite blebs in large minerals (pyroxene and olivine) (Figs. 5e and 5f) implies that they should be recrystallized products rather than melt relics.

AM 037 is clearly the product of melting and recrystallization of chondritic material. Euhedral pyroxene grains surrounded in troilite or Fe-Ni metal are very common in shock melted enstatite chondrites (e.g., Rubin and Wasson 2011), which further confirmed the shock melt origin of AM 037. Chemical compositions of olivine and low-Ca pyroxene are indistinguishable from other AM chondrites collected in the same area (Fig. 10). Relic clasts in AM 037 contain

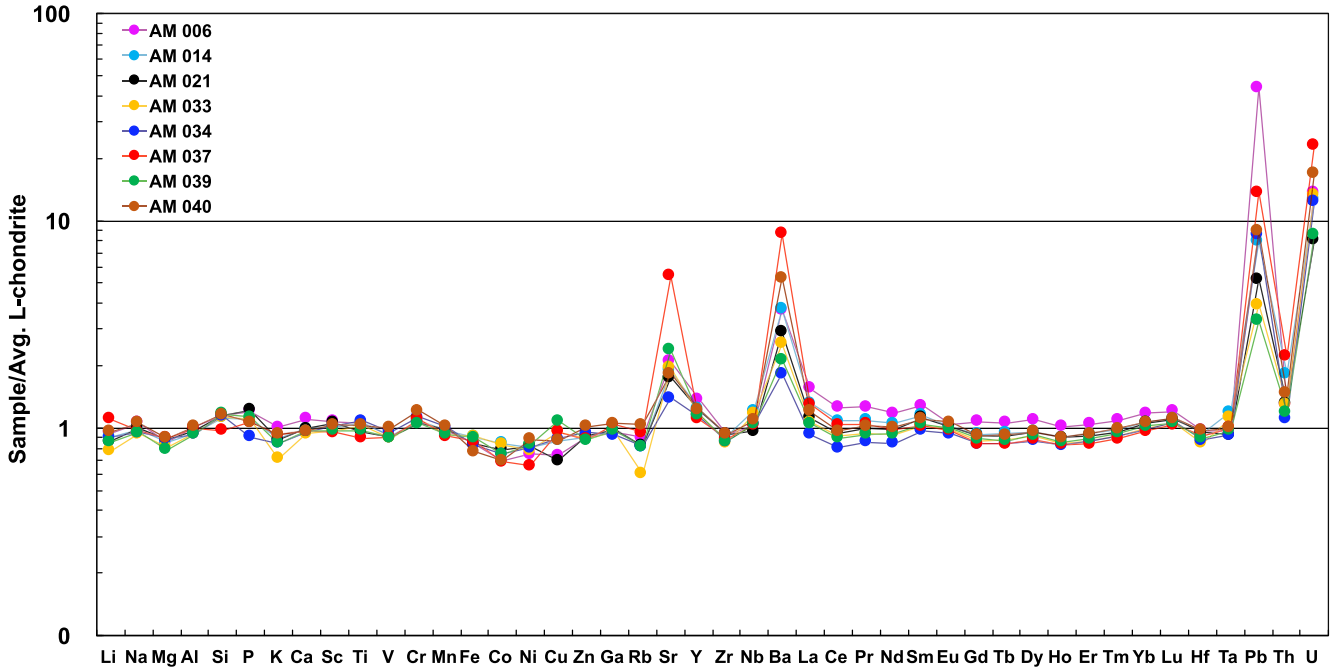

Fig. 8. The elemental distribution patterns of eight AM meteorites normalized to the average L chondrite composition given by Lodders and Fegley (1998). (Color figure can be viewed at wileyonlinelibrary.com.)

Table 3. Oxygen isotopic compositions of AM 029, AM 037, and Jilin meteorites.

Sample	$\delta^{17}O$	1σ	$\delta^{18}O$	1σ	$\Delta^{17}O$	1σ
AM 029	3.69		5.20		0.95	
	3.66		5.10		0.97	
Average	3.67	0.02	5.15	0.07	0.96	0.02
AM 037	3.09		4.20		0.87	
	3.31		4.60		0.88	
Average	3.20	0.15	4.40	0.28	0.88	0.01
Jilin	2.85		4.15		0.70	
	2.97		4.40		0.68	
	2.97		4.31		0.73	
Average	2.93	0.07	4.29	0.13	0.70	0.02

$\Delta^{17}O$ calculated using the formula $\Delta^{17}O' = \delta^{17}O' - 0.528 \times \delta\ ^{18}O'$.

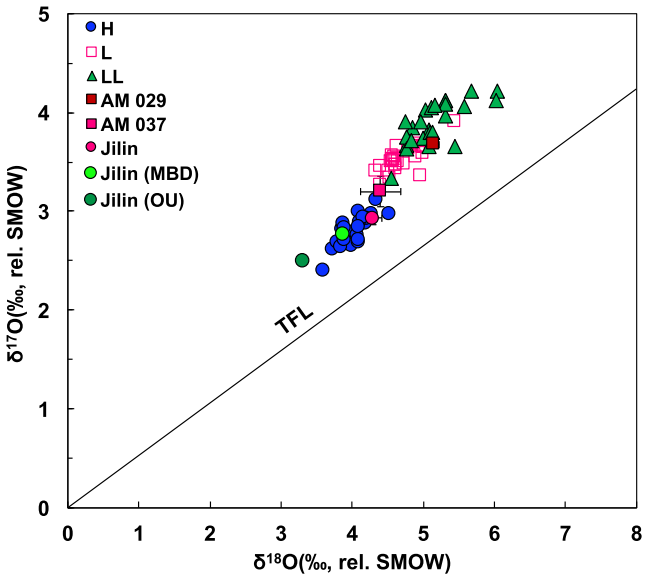

Fig. 9. Bulk oxygen isotopic composition of AM 029 and AM 037 compared to that of other ordinary chondrite groups. All the data except Jilin measured in this study are from Clayton et al. (1991). Jilin (MBD) and Jilin (OU) are reported in Meteoritical Bulletin and Folco et al. (2004). TFL = terrestrial fractionation line. (Color figure can be viewed at wileyonlinelibrary.com.)

abundant tiny blebs of Fe-Ne metal and troilite, which is also coincident with the other AM chondrites (Fig. 3b). The CRE age, ^{4}He, and ^{40}Ar retention ages of AM 037 are well in the range of other chondrites studied here (see Cosmic Ray Exposure Histories and Thermal History sections below). Similar to AM 037, the glassy, lustrous surfaces of some AM meteorite hand specimens indicated that they are melt rocks (e.g., the 24 kg specimen shown in Fig. 2d). Subcentimeter protruding metal nodules can easily be seen on the surface of the 24 kg individual, which is similar to what has been observed on H5-melt breccia Tassédet 004 (MBD). The absence of shock melt veins and rare fractures in the minerals indicates that AM 037 underwent a weak shock (≤S2) after recrystallization. Although the low-Ca pyroxene and olivine compositions

Table 4. Concentrations of He, Ne, and Ar.

			^{3}He	^{4}He	^{20}Ne	^{36}Ar	^{40}Ar			
Sample	Type	Mass(mg)	10^{-8} cm^3 STP/g					^{21}Ne/^{22}Ne	^{20}Ne/^{22}Ne	^{36}Ar/^{38}Ar
AM 006	L5	81.25	10.32 ± 0.09	159.1 ± 1.4	2.94 ± 0.03	6.07 ± 0.09	2082 ± 26	0.913 ± 0.014	0.981 ± 0.015	4.16 ± 0.08
AM 014	L5	56.38	10.88 ± 0.60	168.7 ± 9.3	4.33 ± 0.32	9.70 ± 0.35	3113 ± 94	0.888 ± 0.014	1.227 ± 0.019	4.14 ± 0.15
AM 021	L5	60.05	10.76 ± 0.59	136.2 ± 7.5	3.80 ± 0.28	10.23 ± 0.75	3408 ± 104	0.876 ± 0.013	1.239 ± 0.019	4.23 ± 0.34
AM 024	L5	68.89	13.01 ± 0.36	133.6 ± 3.7	3.33 ± 0.02	3.76 ± 0.24	1298 ± 83	0.907 ± 0.014	0.947 ± 0.015	3.76 ± 0.07
AM 029	L5	76.00	11.58 ± 0.32	139.1 ± 3.9	3.39 ± 0.02	8.09 ± 0.16	2608 ± 35	0.919 ± 0.014	0.967 ± 0.015	4.35 ± 0.08
AM 033	L5	74.28	10.53 ± 0.09	155.6 ± 1.3	2.77 ± 0.03	9.39 ± 0.15	3218 ± 43	0.917 ± 0.014	0.891 ± 0.014	4.48 ± 0.08
AM 034	L5	65.00	12.67 ± 0.12	183.2 ± 1.6	3.94 ± 0.04	3.35 ± 0.06	1651 ± 23	0.912 ± 0.014	0.993 ± 0.015	3.22 ± 0.06
AM 036	L5	48.57	12.29 ± 0.68	180.6 ± 9.9	4.13 ± 0.30	7.40 ± 0.13	2467 ± 75	0.898 ± 0.014	1.054 ± 0.016	4.21 ± 0.08
AM 037	MB	75.00	11.81 ± 0.65	172.1 ± 9.4	3.47 ± 0.25	10.2 ± 0.21	3271 ± 99	0.911 ± 0.014	0.941 ± 0.014	4.55 ± 0.11
AM 039	L5	62.56	10.08 ± 0.25	142.0 ± 3.6	3.18 ± 0.05	8.13 ± 0.11	2702 ± 46	0.893 ± 0.014	1.096 ± 0.017	4.42 ± 0.08
AM 040	L5	58.15	12.20 ± 0.31	162.4 ± 4.1	4.27 ± 0.07	4.13 ± 0.07	2229 ± 39	0.880 ± 0.013	1.179 ± 0.018	3.68 ± 0.10

The given uncertainties (1σ) include the uncertainties of the ion current measurements, the blank corrections, corrections for mass fractionation, and possible uncertainties in the standard calibration (5% for concentrations and 2% for isotope ratios).

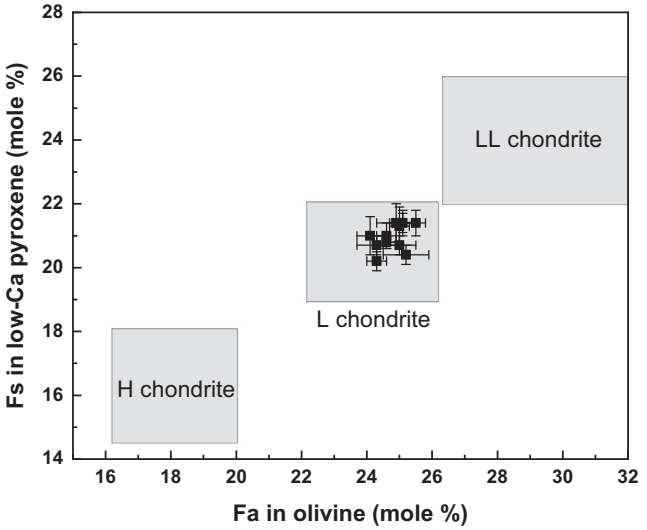

Fig. 10. Olivine fayalite (Fa) versus low-Ca pyroxene ferrosilite (Fs) contents of the studied AM meteorites. Shown uncertainties are 1σ standard deviations. The ranges of Fa and Fs for the H, L, and LL chondrite groups are adopted from Brearley and Jones (1998). Blank squares are AM samples.

are in the range of the other AM specimens, the composition of plagioclase is relatively variable and different to the other AM meteorites (e.g., Or values of plagioclase are 3.8 ± 3.0 mole%, 5.9 ± 1.3 mole%, and 14.0 ± 3.5 mole%, in AM 004, AM 021, and AM 037, respectively). This could be mainly caused by heavy shocks (see Chen and El Goresy 2000).

All the studied meteorites have a very similar whole-rock chemistry (Fig. 8). Except for Mg, Fe, Co, Ni, Sr, Ba, Pb, and U, the studied meteorites have a typical L chondrite composition. Only three small meteorites (AM 006, AM 014, and AM 037) show slight LREE enrichment (Fig. 8), which is similar to the phenomenon observed in ordinary chondrites collected in the Lut Desert, Iran (Pourkhorsandi et al. 2017). Slight REE modification and significant alteration of metal and troilite indicates that the AM meteorites experienced relatively quick weathering (Pourkhorsandi et al. 2017). The observed enrichments and depletions in some elements relative to the average L chondrite group are typical for hot desert ordinary chondrites. The loss of Mg, Fe, Co, and Ni is caused by the oxidation and migration/alteration of these elements during terrestrial weathering (Bland et al. 1998; Crozaz et al. 2003; Al-Kathiri et al. 2005; Hezel et al. 2011). The occurrence of rust on the surface of hot desert ordinary chondrites in contact with the ground is commonly observed (Li et al. 2017a; Du et al. 2021). This is the result of the fluid infiltration from the meteorite's interior to its exterior. Sr, Ba, Pb, and U are fluid mobile elements, and they

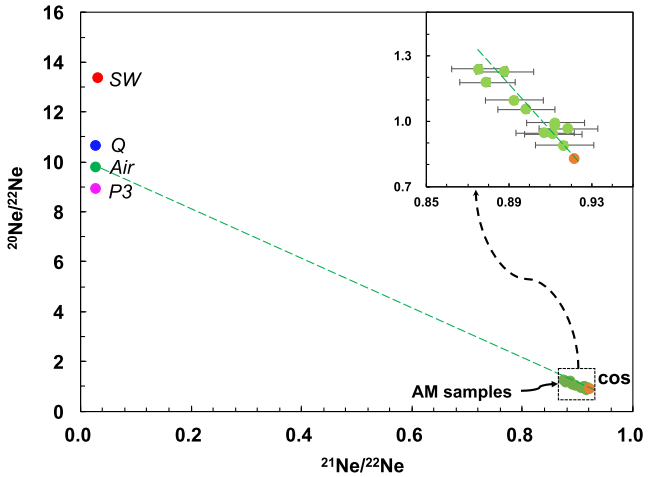

Fig. 11. Neon three-isotope plot of the studied AM meteorites. The data for the AM meteorites plot in a narrow range on the mixing line (dashed line) between cosmogenic (orange circle) and air. The inset upper right hand is a close-up of the data points (green circles). All data plot close to cosmogenic (orange circle), which therefore indicates very small amounts of air. The isotopic compositions of galactic cosmic ray produced Ne (Wieler 2002) and trapped components such as solar wind (SW; Heber et al. 2012), Q (Busemann et al. 2000), P3 (Huss et al. 2003), and atmospheric Ne (Eberhardt et al. 1965) are shown. (Color figure can be viewed at wileyonlinelibrary.com.)

are therefore relatively easy to pick up from the surrounding environment (Al-Kathiri et al. 2005; Hezel et al. 2011; Zurfluh et al. 2016; Pourkhorsandi et al. 2017, 2019). The observed enrichments in these elements in AM meteorites are consistent with this known phenomenon. The Fe-Ni metal in all 12 AM meteorites studied was almost completely oxidized, and troilite showed obvious alteration; no alteration of silicate minerals was observed under SEM. According to the criteria of Wlotzka (1993), the weathering grade of these meteorites is W3.

The whole-rock oxygen isotopic compositions of AM 029 and AM 037 are in the range expected for L chondrites (Fig. 9) (Clayton et al. 1991). However, two data points plot at the two extremities of the area covered by L chondrite. The relatively lighter oxygen isotopic composition of AM 037 might partly be due to the contamination with terrestrial oxygen. Indeed, the oxygen isotopic composition (i.e., $\delta^{18}O$: −9‰ to −10‰) of rainfall in the AM meteorite collection region is lighter than that of typical L chondrite (Luo et al. [2008] and references therein). However, we cannot rule out the possibility of an inhomogeneous oxygen isotopic composition for this meteoroid. In fact, inhomogeneity of oxygen isotopic compositions in Jilin meteorite might exist (Fig. 9) (Jilin meteorite in MBD; Folco et al. 2004).

Sulfidization Reaction in AM 034

In some of the low-Ca pyroxene grains found in AM 034 that are located in the troilite–pyroxene (low-Ca)–olivine intergrowth (TPOI), Fe and Ca contents are lower than in the low-Ca pyroxene located in other parts of AM 034 but also in other studied meteorites (Figs. 6 and 7). As discussed above, AM 034 is a type 5 chondrite and the chemical composition of low-Ca pyroxene should have been homogenized during the thermal metamorphism process. It is most likely that the Fe depleted low-Ca pyroxene in AM 034 is a secondary product formed in a shock event. Similar intergrowths were observed in acapulcoites (El Goresy et al. 2005), brachinites (and brachinite-like) achondrites (Rumble et al. 2008; Goodrich et al. 2011, 2017; Irving et al. 2013), HED meteorite (Patzer and McSween 2012; Zhang et al. 2018, 2020), and Apollo lunar sample (Norman 1981; Lindstrom and Salpas 1983). Several mechanisms were proposed to explain the formation of a TPOI or a TPOI-like assemblage, including (1) crystallization of a sulfide-silicate partial melt (El Goresy et al. 2005), (2) quenching of the shock-induced melt that is a mixture of orthopyroxene and troilite (Patzer and McSween 2012), (3) methane infiltration and reduction of olivine (Irving et al. 2013), and (4) sulfidization of primary olivine by an S-rich fluid/gas (Colson 1992; Norman et al. 1995; Shearer et al. 2012; Singerling et al. 2013; Zhang et al. 2018, 2020).

All shock melt veins and shock melt pockets in AM 034 contain plagioclase melt (Figs. 5e–h); however, the TPOI does not (Fig. 6). Therefore, scenarios (1) and (2) are rather unlikely. The formation of the TPOI via methane or C reduction of olivine is also not possible as this would produce a considerable amount of metal in the assemblage. In the TPOI of AM 034, Fe metal is not observed. The most plausible explanation for the formation of the TPOI is therefore sulfidization of primary olivine by S vapors. The reaction of olivine and S vapor was experimentally confirmed by Kullerud and Yoder (1963). The production of S vapor is possible via the high-temperature breakdown of troilite (Rubin et al. 1999; Shearer et al. 2012). Heating a eucrite at 800–900 °C can significantly increase the S_2 partial pressure (Palme et al. 1988). For AM 034, the heavy impact can have generated enough heat to reach the breakdown temperature of troilite. High-temperature S vapor might have subsequently entered the cracks in olivine resulting in sulfidization (Singerling et al. 2013), for example,

$$2(Fe, Mg)_2SiO_4 + S_2 \rightarrow 2MgSiO_3 + 2FeS + O_2(g).$$

Table 5. Cosmogenic (c), trapped (tr), and radiogenic (rad) noble gases concentrations and isotopic ratios

Sample	Type	Mass(mg)	$^{3}He_{c}$	$^{21}Ne_{c}$	$^{38}Ar_{c}$	$^{4}He_{rad}$	$^{36}Ar_{tr}$	$^{40}Ar_{rad}$	$(^{22}Ne/^{21}Ne)_{c}$
			10^{-8} cm^3 STP/g						
AM 006	L5	81.25	10.32 ± 0.09	2.735 ± 0.033	0.359 ± 0.006	97.5 ± 1.4	5.84 ± 0.09	356 ± 5	1.075 ± 0.016
AM 014	L5	56.38	10.88 ± 0.60	3.128 ± 0.230	0.589 ± 0.020	103.4 ± 9.9	9.33 ± 0.34	357 ± 11	1.074 ± 0.017
AM 021	L5	60.05	10.76 ± 0.59	2.679 ± 0.197	0.560 ± 0.027	71.6 ± 8.3	9.87 ± 0.72	491 ± 15	1.088 ± 0.017
AM 024	L5	68.89	13.01 ± 0.36	3.189 ± 0.028	0.333 ± 0.022	55.6 ± 4.3	3.55 ± 0.23	248 ± 16	1.085 ± 0.017
AM 029	L5	76.00	11.58 ± 0.32	3.218 ± 0.028	0.385 ± 0.009	69.6 ± 4.3	7.85 ± 0.16	288 ± 4	1.069 ± 0.017
AM 033	L5	74.28	10.53 ± 0.09	2.853 ± 0.036	0.377 ± 0.006	92.4 ± 1.4	9.15 ± 0.14	513 ± 7	1.080 ± 0.017
AM 034	L5	65.00	12.67 ± 0.12	3.617 ± 0.043	0.465 ± 0.008	107.2 ± 1.7	3.05 ± 0.06	748 ± 10	1.073 ± 0.016
AM 036	L5	48.57	12.29 ± 0.68	3.518 ± 0.258	0.418 ± 0.014	106.9 ± 10.7	7.14 ± 0.12	357 ± 11	1.083 ± 0.017
AM 037	MB	75.00	11.81 ± 0.65	3.360 ± 0.247	0.369 ± 0.013	101.2 ± 10.2	9.97 ± 0.20	324 ± 10	1.081 ± 0.016
AM 039	L5	62.56	10.08 ± 0.25	2.588 ± 0.045	0.354 ± 0.005	81.5 ± 3.9	7.91 ± 0.10	365 ± 6	1.085 ± 0.017
AM 040	L5	58.15	12.20 ± 0.31	3.182 ± 0.053	0.393 ± 0.008	89.2 ± 4.5	3.89 ± 0.07	1081 ± 19	1.091 ± 0.017

Table 6. Cosmic ray exposure ages (Ma) and gas retention ages (Ma) of the measured samples.

	Type	Mass(mg)	P3	P21	P38	T_3	T_{21}	T_{38}	T_4	T_{40}
AM 006	L5	81.25	1.628	0.433	0.051	6.3 ± 1.9	6.3 ± 1.9	7.0 ± 2.1	313 ± 4	798 ± 10
AM 014	L5	56.38	1.628	0.433	0.051	6.7 ± 2.0	7.2 ± 2.2	11.5 ± 3.5	332 ± 31	887 ± 27
AM 021	L5	60.05	1.622	0.403	0.048	6.6 ± 2.0	6.6 ± 2.1	11.6 ± 3.5	232 ± 26	1145 ± 35
AM 024	L5	68.89	1.624	0.411	0.049	8.0 ± 2.4	7.8 ± 2.3	6.8 ± 2.1	180 ± 13	666 ± 43
AM 029	L5	76.00	1.630	0.446	0.053	7.1 ± 2.1	7.2 ± 2.2	7.3 ± 2.2	262 ± 14	758 ± 10
AM 033	L5	74.28	1.626	0.421	0.050	6.5 ± 1.9	6.8 ± 2.0	7.5 ± 2.3	298 ± 4	1370 ± 18
AM 034	L5	65.00	1.629	0.436	0.052	7.8 ± 2.3	8.3 ± 2.5	9.0 ± 2.7	344 ± 5	1578 ± 22
AM 036	L5	48.57	1.624	0.415	0.050	7.6 ± 2.3	8.5 ± 2.6	8.4 ± 2.5	244 ± 34	897 ± 27
AM 037	MB	75.00	1.625	0.420	0.050	7.3 ± 2.2	8.0 ± 2.5	7.4 ± 2.2	325 ± 32	791 ± 24
AM 039	L5	62.56	1.624	0.411	0.049	6.2 ± 1.9	6.3 ± 1.9	7.2 ± 2.2	263 ± 12	938 ± 16
AM 040	L5	58.15	1.621	0.398	0.048	7.5 ± 2.3	8.0 ± 2.4	8.2 ± 2.5	288 ± 14	1879 ± 33

The errors on T_4 and T_{40} are only calculated based on errors of ^{4}He and ^{40}Ar concentrations.

Most low-Ca pyroxene in the TPOI in AM 034 is Fe and Ca depleted compared to the normal occurrences in AM 034 and other AM samples (Fig. 6). This might be due to partial recombination of Fe into FeS during the sulfidization process. Following the discussion above, we propose that the TPOI in AM 034 has been formed via sulfidization. However, we cannot completely rule out the crystallization of a sulfide-silicate partial melt; a scenario originally proposed by El Goresy et al. (2005).

Cosmic Ray Exposure Histories

Primitive chondrites contain noble gases of different origins, for example, "primordial" (HL, G, and N from presolar grains, and Q gas), solar gas, radiogenic, and cosmogenic gases (Huss et al. 1996; Choi et al. 2018). Compared to primitive chondrites, higher petrographic types usually contain fewer noble gas components because most of the original noble gases have been lost via thermal metamorphism (Zähringer 1968; Alaerts et al. 1979; Sears and Hasan 1987; Choi et al. 2018). The neon three-isotope plot (i.e., $^{20}Ne/^{22}Ne$ versus $^{21}Ne/^{22}Ne$) is commonly used to determine shielding conditions and identify the different components contributing to the measured noble gases (Leya et al. 2013; Füri et al. 2020; Smith et al. 2020). In the neon 3-isotope plot of AM samples (Fig. 11), the data plot along a mixing line between cosmogenic ($^{20}Ne/^{22}Ne = 0.83$; $^{21}Ne/^{22}Ne = 0.92$) and an endmember with a high $^{20}Ne/^{22}Ne$ ratio and low $^{21}Ne/^{22}Ne$ ratio, which is most likely atmospheric contamination ($^{20}Ne/^{22}Ne = 9.8$; $^{21}Ne/^{22}Ne = 0.029$). The presence of only atmospheric gases is consistent with the high petrographic type (absence of other trapped components) and the strong weathering degree of the AM meteorites. Cosmogenic $^{21}Ne_{cos}$ concentrations were determined using a classical two-component deconvolution (cosmogenic and air).

Measured $^{36}Ar/^{38}Ar$ ratios range from 3.22 ± 0.06 to 4.55 ± 0.11, indicating that measured Ar is a mixture of cosmogenic and trapped, the latter again most likely

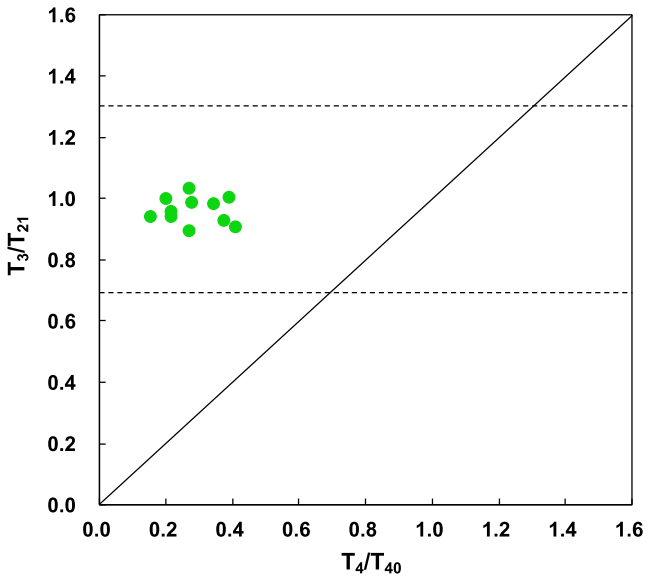

Fig. 12. Plot of T_4/T_{40} versus T_3/T_{21} of the 11 studied AM meteorites. The ratios of T_3/T_{21} are all close to 1, indicating no noble gas lost during cosmic ray exposure. The ratios of T_4/T_{40} are <0.5, implying significant loss of radiogenic noble gases, either of ^{4}He only or of both ^{4}He and ^{40}Ar. (Color figure can be viewed at wileyonlinelibrary.com.)

atmospheric contamination. Cosmogenic $^{38}Ar_{cos}$ concentrations were calculated by assuming a two-component mixture between air ($^{36}Ar/^{38}Ar = 5.32$) and cosmogenic ($^{36}Ar/^{38}Ar = 0.63$).

For He, we assumed that measured ^{3}He is entirely cosmogenic, which is a safe assumption considering the high petrographic type of the studied meteorites. The amount of cosmogenic $^4He_{cos}$ is calculated as follows (Leya and Masarik 2009):

$$^4He_{meas} = {}^4He_{rad} + (^4He/^3He)_{cos} \times {}^3He_{cos}.$$

We assumed that $(^4He/^3He)_{cos}$ ~6 × $^3He_{cos}$ (e.g., Leya and Masarik 2009).

The cosmogenic noble gas concentrations are reported in Table 5. We calculated the CRE ages of the studied meteorites based on cosmogenic $^3He_{cos}$, $^{21}Ne_{cos}$, and $^{38}Ar_{cos}$ contents and the empirical formulas given by Eugster (1988; for ^{3}He age [T_3]) and by Dalcher et al. (2013; for ^{21}Ne [T_{21}] and ^{38}Ar [T_{38}] ages) (Table 6). Except for T_{38} of AM 014 (11.5 ± 3.5 Ma) and AM 021 (11.6 ± 3.5 Ma), the CRE ages for all meteorites and for all considered cosmogenic nuclides are in a relatively narrow range from 6.2 ± 1.9 Ma to 9.0 ± 2.7 Ma. The similar CRE ages for the meteorites further confirm that they are paired. The average CRE age is 7.6 ± 1.3 Ma. To date, there is no estimate of the surface age in the collection area of the Kumtag desert. Considering that terrestrial ages of ordinary chondrites in the hot desert are typically in the range of ka but not Ma (Al-Kathiri et al. 2005; Gnos et al. 2009; Gattacceca et al. 2011), the CRE age is therefore also very close to the ejection age.

Thermal History

As discussed above, AM meteorites experienced different degrees of impact melting and then underwent recrystallization. Such processes are expected to be related to a partial or total loss of radiogenic gases ($^4He_{rad}$ and $^{40}Ar_{rad}$). Consequently, the T_4 and T_{40} ages can reveal the thermal history of a meteorite. We obtained the concentrations of radiogenic $^4He_{rad}$ and $^{40}Ar_{rad}$ using the deconvolution procedures described above (Table 5). The $^4He_{rad}$ and $^{40}Ar_{rad}$ concentrations among the samples vary by a factor of ~3, thus indicating a different degree of noble gas losses assuming equal parent isotope concentrations. For calculating the ^{40}Ar retention ages (T_{40}), the K content of each individual AM sample listed in Table 2 was used. For calculating ^{4}He retention ages (T_4), we use the average U, Th, and Sm contents (15, 42, and 203 ng g^{-1}, respectively) of L chondrites as given by Lodders and Fegley (1998). We rather use the average values for L chondrites and not the individual U, Th, and Sm concentrations measured by us because AM samples are significantly enriched in U and Th, and slightly enriched in Sm by terrestrial weathering. Among the measured 11 meteorites, AM 024 and AM 034 have the lowest and highest T_4 ages of 180 and 344 Ma, respectively. For T_{40}, AM 024 and AM 040 have the lowest and highest ages of 666 and 1879 Ma, respectively. While the T_3/T_{21} ratios are in the range of 0.89–1.03, the T_4/T_{40} ratios are in the range of 0.15–0.39 (Fig. 12). This indicates that, first, there was no or only very minor noble gas loss during CRE but that, second, there was a significant noble gas loss on the parent asteroid. The scatter in the T_4/T_{40} ratios indicates the different extent of noble gas losses in the different samples. Although we studied only individual AM 037 for shock features, we did not observe any indication for shock stage higher than S3. Consequently, it is possible that none of the samples experienced a heating event after they cooled after the impact. In such a simple scenario, we would expect a T_4/T_{40} ratio of ~1 for AM 037, which is not the case. This is in contradiction with the petrographic characteristics of AM 037, which is a recrystallized chondrule-free rock, containing only 5 vol% of relict clasts (also significantly affected by high temperature) (Fig. 3b). An underestimation of the K contents in the AM 037 sample might be the possible reason for such differences. At least, the enrichment in K in feldspar glass of AM 037 has been detected by EPMA measurement (Table S1). Anyway, the fact that AM 037 is almost completely melted (which, in

turn, could possibly completely degas the noble gases) indicates that the gas retention age of this sample represents the possible time of the impact melt of the meteorites. We prefer to use T_4 (325 Ma) of AM 037 as the impact melt time of these meteorites. A heavy shock event and breakup event on L-chondrite parent body around 470 Ma were widely reported (Nakamura et al. 1990; Fujiwara and Nakamura 1992; Korochantseva et al. 2007; Weirich et al. 2012; Yin et al. 2014; S. L. Li and Hsu 2018; Y. Li and Hsu 2018; Wu and Hsu 2019). It is not sure whether the impact melt event of AM samples belongs to 470 Ma shock event or reflects a younger impact event. Therefore, in order to obtain a more accurate impact time, Ar-Ar dating of AM 037 is needed.

CONCLUSIONS

The AM meteorites originated from a single meteorite shower; the incoming direction of the meteoroid was from southwest to northeast with a relatively large incoming angle. The strewn field has a width of ~5 km and a length of ~10 km. Hundreds of meteorite samples were collected in this strewn field, with masses ranging from several grams to 24 kg; the total mass is more than 100 kg.

The oxygen isotope data (AM 029: $5.15 \pm 0.07‰$, $3.67 \pm 0.02‰$, and $0.96 \pm 0.02‰$; AM 037: $4.40 \pm 0.28‰$, $3.20 \pm 0.15‰$, and $0.88 \pm 0.01‰$), together with the mineralogical information, clearly indicate that AM meteorites are L5 ordinary chondrites. The average Fa and Fs values of these specimens range from 24.1 ± 0.4 to 25.0 ± 0.5 mole% and from 20.2 ± 0.3 to 21.4 ± 0.6 mole%, respectively.

The meteorites experienced a heavy impact as shock-induced fractures, shock veins, and shock melt pockets are commonly seen. Many fractures seen in minerals are filled with shock melts of troilite and feldspar. Densely scattered troilite dots in olivine and pyroxene were produced by the heavy impact. Some meteorites in this strewn field are shock melt rocks, including the largest fragment (~24 kg). The gas retention ages indicate that the strong impact leading to the melting event occurred 320 Ma ago, though this age is highly uncertain. The impact might have also caused the decomposition of troilite, and the sulfur vapor generated by this process, in turn, might have vulcanized one olivine grain in AM 034. In addition, due to the shock, there is now a relatively large variation in the chemical composition of plagioclase, that is, An and Or values are in the range of 4.0 ± 0.3–22.1 ± 2.9 mole% and 2.5 ± 0.8–12.1 ± 2.1 mole%, respectively. The CRE ages of AM meteorites vary between 6.2 ± 1.9 Ma and 9.0 ± 2.7 Ma; the average CRE age is 7.6 ± 1.3 Ma. Assuming a reasonable terrestrial age of a few ka, typical for hot desert meteorites (Al-Kathiri et al. 2005; Gnos et al. 2009; Gattacceca et al. 2011), the AM meteorite was most likely ejected around 7 Ma.

Similar to ordinary chondrites collected in other hot deserts, the bulk chemical compositions of AM meteorites were altered during their terrestrial residence. Mg, Fe, Co, and Ni in AM meteorites migrated into the surrounding soils, while Sr, Ba, Pb, and U were picked up by the meteorite from the soil. The weathering degree of the meteorites is W3.

Acknowledgments—This work was supported by the Strategic Priority Research Program of the Chinese Academy of Science, Grant No. XDB41000000 and the Chinese Academy of Sciences "Light of West China" Program (Shijie Li, 2019) and the Swiss National Science Foundations (IL: 200021_159562). The authors thank all members of the 2013 AM meteorite hunting campaign. We are grateful to meteorite hunters Peng Wang, Changling Wang, and Kexin Yang for providing much valuable information about the AM meteorite strewn field. We thank Hans-Erich Jenni, Dr. Peter Stephenson, Dr. Antoine Roth, Dr. Ramakrishna Ramisetty, and Patrick Enderli at the University of Bern for their help during noble gas measurements. And we thank Dr. Lanfang Xie from the Guilin University of Technology for her assistance in the EMPA lab. Finally, we appreciate valuable comments by reviewers K. Welten, P. Heck, and G. Herzog.

Data Availability Statement—All data generated or analyzed during this study are included in this article.

Editorial Handling—Dr. Marc Caffee

REFERENCES

Alaerts L., Lewis R. S., and Anders E. 1979. Isotopic anomalies of noble gases in meteorites and their origins—III. LL-chondrites. *Geochimica et Cosmochimica Acta* 43:1399–1425.

Al-Kathiri A., Hofmann B. D., Jull A. J. T., and Gnos E. 2005. Weathering of meteorites from Oman: Correlation of chemical and mineralogical weathering proxies with ^{14}C terrestrial ages and the influence of soil chemistry. *Meteoritics & Planetary Science* 40:1215–1239.

Bland P. A., Sexton A. S., Jull A. J. T., Bevan A. W. R., Berry F. J., Thornley D. M., Astin T. R., Britt D. T., and Pillinger C. T. 1998. Climate and rock weathering: A study of terrestrial age dated ordinary chondritic meteorites from hot desert regions. *Geochimica et Cosmochimica Acta* 62:3169–3184.

Brearley A. J. and Jones R. H. 1998. Chondritic meteorites. In *Planetary materials*, vol. 36, edited by Papike J. J. Washington, D.C.: Mineralogical Society of America. pp. 3-1–3-398.

Busemann H., Baur H., and Wieler R. 2000. Primordial noble gases in "phase Q" in carbonaceous and ordinary chondrites studied by closed-system stepped etching. *Meteoritics & Planetary Science* 35:949–973.

Chen M. and El Goresy A. 2000. The nature of maskelynite in shocked meteorites: Not diaplectic glass but a glass quenched from shock-induced dense melt at high pressures. *Earth and Planetary Science Letters* 179:489–502.

Choi J., Nagao K., Baek J. M., and Lee J. I. 2018. Effect of thermal metamorphism on noble gas of carbonaceous chondrites: Comparison of Vigarano (CV3) and Maraliga (CK4) (abstract #1940). 49th Lunar and Planetary Science Conference. CD-ROM.

Clayton R. N., Mayeda T. K., Goswami J. N., and Olsen E. J. 1991. Oxygen isotope studies of ordinary chondrites. *Geochimica et Cosmochimica Acta* 55:2317–2337.

Colson R. O. 1992. Mineralization on the Moon? Theoretical considerations of Apollo 16 "rusty rocks," sulfide replacement in 67016, and surface-correlated volatiles on lunar volcanic glass. Proceedings, 22nd Lunar and Planetary Science Conference. pp. 427–436.

Crozaz G., Floss C., and Wadhwa M. 2003. Chemical alteration and REE mobilization in meteorites from hot and cold deserts. *Geochimica et Cosmochimica Acta* 67:4727–4741.

Dalcher N., Caffee M. W., Nishiizumi K., Welten K. C., Vogel N., Wieler R., and Leya I. 2013. Calibration of cosmogenic noble gas production in ordinary chondrites based on ^{36}Cl-^{36}Ar ages. Part 1: Refined produced rate for cosmogenic ^{21}Ne and ^{38}Ar. *Meteoritics & Planetary Science* 48:1841–1862.

Du K., Li S. J., Leya I., Smith T., Zhang D. L., and Wang P. 2021. The Kumtage meteorite strewn field. *Advances in Space Research* 67:4089–4098.

El Goresy A., Zinner E., Pellas P., and Caillet C. 2005. A menagerie of graphite morphologies in the Acapulco meteorite with diverse carbon and nitrogen isotopic signatures: Implications for the evolution history of acapulcoite meteorites. *Geochimica et Cosmochimica Acta* 69:4535–4556.

Eberhardt P., Eugster O., and Marti K. 1965. A redetermination of the isotopic composition of atmospheric neon. *Zeitschrift für Naturforschung* 20a:623–624.

Eugster O. 1988. Cosmic-ray production rates for ^{3}He, ^{21}Ne, ^{38}Ar, ^{83}Kr, and ^{126}Xe in chondrites based on ^{81}Kr-Kr ages. *Geochimica et Cosmochimia Acta* 52:1649–1662.

Folco L., Bland P. A., D'Orazio M., Franchi I. A., Kelley S. P., and Rocchi S. 2004. Extensive impact melting on the H-chondrite parent asteroid during the cataclysmic bombardment of the early solar system: Evidence from the achondritic meteorite Dar al Gani 896. *Geochimica et Cosmochimia Acta* 68:2379–2397.

Fujiwara T. and Nakamura N. 1992. Additional evidence of a young impact-melting event on the L-chondrite parent body (abstract). 23rd Lunar and Planetary Science Conference. p. 387.

Füri E., Zimmermann L., Deloule E., and Trappitsch E. 2020. Cosmic ray effects on the isotope composition of hydrogen and noble gases in lunar samples: Insights from Apollo 12018. *Earth and Planetary Science Letters* 550:116550.

Gattacceca J., Valenzuela M., Uehara M., Jull A. J. T., Giscard M., Rochette P., Braucher R., Suavet C., Gounelle M., Morata D., Munayco P., Bourot-Denise M., Bourles D., and Demory F. 2011. The densest meteorite collection area in hot deserts: The San Juan meteorite field (Atacama Desert, Chile). *Meteoritics & Planetary Science* 46:1276–1287.

Gnos E., Lorenzetti S., Eugster O., Jull A. J. T., Hofmann B. A., Al-Khatiri A., and Eggimann M. 2009. The Jiddat al Harasis 073 strewn field, Sultanate of Oman. *Meteoritics & Planetary Science* 44:375–387.

Goodrich C. A., Kita N. T., Spicuzza M. J., Valley J. W., Zipfel J., Mikouchi T., and Miyamoto M. 2011. The Northwest Africa 1500 meteorite: Not a ureilite, maybe a brachinite. *Meteoritics & Planetary Science* 45:1906–1928.

Goodrich C. A., Kita N. T., Sutton S. R., Wirick S., and Gross J. 2017. The Miller Range 090340 and 090206 meteorites: Identification of new brachinite-like achondrites with implications for the diversity and petrogenesis of the brachinite clan. *Meteoritics & Planetary Science* 52:949–978.

Heber V. S., Baur H., Bochsler P., McKeegan K. D., Neugebauer M., Reisenfeld D. B., Wieler R., and Wiens R. C. 2012. Isotopic mass fractionation of solar wind: Evidence from fast and slow solar wind collected by the genesis mission. *The Astrophysical Journal* 759:121.

Hezel D. C., Schlüter J., Kallweit H., Jull A. J. T., Al Fakeer O. Y., Al Shamsi M., and Strekopytov S. 2011. Meteorites from the United Arab Emirates: Description, weathering, and terrestrial ages. *Meteoritics & Planetary Science* 46:327–336.

Huss G. R., Lewis R. S., and Hemkin S. 1996. The "normal planetary" noble gas component in primitive chondrites: Compositions, carrier, and metamorphic history. *Geochimica et Cosmochimica Acta* 60:3311–3340.

Huss G. R., Meshik A. P., Smith J. B., and Hohenberg C. M. 2003. Presolar diamond, silicon carbide, and graphite in carbonaceous chondrites: Implications for thermal processing in the solar nebula. *Geochimica et Cosmochimica Acta* 67:4823–4848.

Irving A. J., Kuehner S. M., and Ziegler K. 2013. Petrology and oxygen isotopic composition of brachinite-like achondrites Northwest Africa 7388 and Northwest Africa 7605, and evidence for late-stage methane-triggered reduction (abstract #2192). 44th Lunar and Planetary Science Conference. CD-ROM.

Korochantseva E. V., Trieloff M., Lorenz C. A., Buykin A. I., Ivanova M. A., Schwarz W. H., Hopp J., and Jessberger E. K. 2007. L-chondrite asteroid breakup tied to Ordovician meteorite shower by multiple isochron ^{40}Ar-^{39}Ar dating. *Meteoritics & Planetary Science* 42:113–130.

Kullerud G. and Yoder H. S. Jr. 1963. *Sulfide-silicate reactions*. Washington, D.C.: Carnegie Institution of Washington Yearbook. pp. 215–218.

Leya I. and Masarik J. 2009. Cosmogenic nuclides in stony meteorites revisited. *Meteoritics & Planetary Science* 44:1061–1086.

Leya I., Ammon K., Cosarinsky M., Dalcher N., Gnos E., Hofmann B., and Huber L. 2013. Light noble gases in 12 meteorites from the Omani desert, Australia, Mauritania, Canada, and Sweden. *Meteoritics & Planetary Science* 48:1401–1414.

Li S. J., Wang S. J., Bao H. M., Miao B. K., Liu S., Coulson I. M., Li X. Y., and Li Y. 2011. The Antarctic achondrite, Grove Mountains 021663: An olivine-rich winonaite. *Meteoritics & Planetary Science* 46:1329–1344.

Li S. J., Wang S., Leya I., Smith T., Tang J., Wang P., Zeng X., and Li Y. 2017a. A chondrite strewn field was found in The Kumtag 016 L5 strewn field 1129 east of Lop Nor, Xinjiang (in Chinese). *Chinese Science Bulletin* 62:2407–2415.

Li S. J., Wang S. J., Leya I., Li Y., Li X. Y., and Smith T. 2017b. Petrology, mineralogy, porosity, and cosmic-ray exposure history of Huaxi ordinary chondrite. *Meteoritics & Planetary Science* 52:937–948.

Li S. J., Yin Q.-Z., Bao H. M., Sanborn M. E., Irving A., Ziegler K., Agee C., Marti K., Miao B. K., Li X. Y., Li Y., and Wang S. J. 2018. Evidence for a multilayered internal structure of the chondritic acapulcoite-lodranite parent asteroid. *Geochimica et Cosmochimica Acta* 242:82–101.

Li S. L. and Hsu W. B. 2014. New dense meteorite collection areas were found in Lop Nur, Xinjiang (in Chinese). *Chinese Science Bulletin* 59:2091–2097.

Li S. L. and Hsu W.-B. 2018. The nature of the L chondrite parent body's disruption as deduced from high-pressure phases in the Sixiangkou L6 chondrite. *Meteoritics & Planetary Science* 53:2107–2122.

Li Y. and Hsu W.-B. 2018. Multiple impact events on the L-chondritic parent body: Insights from SIMS U-Pb dating of Ca-phosphates in the NWA 7251 L-melt breccia. *Meteoritics & Planetary Science* 53:1081–1095.

Lindstrom M. M., and Salpas P. A. 1983. Geochemical studies of feldspathic fragmental breccias and the nature of north ray crater ejecta. Proceedings, 13th Lunar and Planetary Science Conference. *Journal of Geophysical Research* 88: A671–A683.

Lodders K. and Fegley B. 1998. *The planetary scientist's companion*. New York: Oxford University Press. p. 371p.

Luo W. J., Wang S. J., and Liu X. M. 2008. Regional characteristics of modern precipitation ^{18}O values and implications for paleoclimate research in China (in Chinese). *Earth and Environment* 36:47–55.

Nakamura N., Fujiwara T., and Nohda S. 1990. Young asteroid melting event indicated by Rb-Sr dating of the Point of Rocks meteorite. *Nature* 345:51–52.

Norman M. D. 1981. Petrology of suevitic lunar breccia 67016. Proceedings, 12th Lunar and Planetary Science Conference. pp. 235–252.

Norman M. D., Keil K., Griffin W. L., and Ryan C. G. 1995. Fragments of ancient lunar crust: Petrology and geochemistry of ferroan noritic anorthosites from the Descartes region of the Moon. *Geochimica et Cosmochimica Acta* 59:831–847.

Palme H., Wlotzka F., Spettel B., Dreibus G., and Weber H. 1988. Camel Donga: A eucrite with high metal content. *Meteoritics* 23:49–57.

Patzer A. and McSween H. Y. Jr. 2012. Ordinary (mesostasis) and not-so-ordinary (symplectites) late-stage assemblages in howardites. *Meteoritics & Planetary Science* 47:1475–1490.

Pourkhorsandi H., D'Orazio M., Rochette P., Valenzuela M., Gattacceca J., Mirnejad H., Sutter B., Hutzler A., and Aboulahris M. 2017. Modification of REE distribution of ordinary chondrites from Atacama (Chile) and Lut (Iran) hot deserts: Insights into the chemical weathering of meteorites. *Meteoritics & Planetary Science* 52:1843–1858.

Pourkhorsandi H., Gattacceca J., Rochette P., D'Orazio M., Kamali H., Avillez R., Letichevsky S., Djamali M., Mirnejad H., Debaille V., and Jull A. J. T. 2019. Meteorites from the Lut Desert (Iran). *Meteoritics & Planetary Science* 54:1737–1763.

Rubin A. E. and Wasson J. T. 2011. Shock effects in "EH6" enstatite chondrites and implications for collisional heating of the EH and EL parent asteroids. *Geochimica et Cosmochimica Acta* 75:3757–4780.

Rubin A. E., Sailer A. L., and Wasson J. T. 1999. Troilite in the chondrules of type-3 ordinary chondrites: Implications for chondrule formation. *Geochimica et Cosmochimica Acta* 63:2281–2298.

Rumble D. III, Irving A. J., Bunch T. E., Wittke J. H., and Kuehner S. M. 2008. Oxygen isotopic and petrological diversity among brachinites NWA 4872, NWA 4874, NWA 4882 and NWA 4969: How many ancient parent bodies? (abstract #1974). 39th Lunar and Planetary Science Conference. CD-ROM.

Sears D. W. G. and Hasan F. A. 1987. The type three ordinary chondrites: A review. *Surveys in Geophysics* 9:43–97.

Shearer C. K., Burger P. V., Guan Y., Papike J. J., Sutton S. R., and Atudorei N.-V. 2012. Origin of sulfide replacement textures in lunar breccias. Implications for vapor element transport in the lunar crust. *Geochimica et Cosmochimica Acta* 83:138–158.

Singerling S. A., McCoy T. J., and Gardner-Vandy K. G. 2013. Possible evidence for sulfidization reactions in the Miller Range brachinites(?) (abstract #1669). 44th Lunar and Planetary Science Conference. CD-ROM.

Smith T., Ranjith P. M., He H., and Zhu R. X. 2020. Reviewing Martian atmospheric noble gas measurements: From Martian meteorites to Mars missions. *Geosciences* 10:439.

Stoffler D., Keil K., and Scott E. R. D. 1991. Shock metamorphism of ordinary chondrites. *Geochimica et Cosmochimica Acta* 55:3845–3867.

Weirich J. R., Swindle T. D., and Isachsen C. E. 2012. ^{40}Ar-^{39}Ar age of Northwest Africa 091: More evidence for a link between L chondrites and fossil meteorites. *Meteoritics & Planetary Science* 47:1324–1335.

Wieler R. 2002. Cosmic-ray-produced noble gases in meteorites. In *Noble gases in geochemistry and cosmochemistry*, edited by Porcelli D., Ballentine C. J., and Wieler R. *Reviews in Mineralogy and Geochemistry* 47:125–170.

Wlotzka F. 1993. A weathering scale for the ordinary chondrites. *Meteoritics* 28:460.

Wu Y. and Hsu W. 2019. Petrogenesis and in situ U-Pb geochronology of a strongly shocked L-melt rock Northwest Africa 11042. *Journal of Geophysical Research: Planets* 124:893–909.

Yin Q.-Z., Zhou Q., Li Q.-L., Li X.-H., Liu Y., Tang G.-Q., Krot A. N., and Jenniskens P. 2014. Records of the Moon-forming impact and the 470 Ma disruption of the L chondrite parent body in the asteroid belt from U-Pb apatite ages of Novato (L6). *Meteoritics & Planetary Science* 49:1426–1439.

Zähringer J. 1968. Rare gases in stony meteorites. *Geochimica et Cosmochimica Acta* 32:209–237.

Zeng X. J., Li S. J., Leya I., Wang S. J., Smith T., Li Y., and Wang P. 2018. The Kumtag 015 L5 strewn field, Xinjiang of China. *Meteoritics & Planetary Science* 53:1113–1130.

Zhang A. C., Bu Y. F., Pang R. L., Sakamoto N., Yurimoto H., Chen L. H., Gao J. F., Du D. H., Wang X. L., and Wang R. C. 2018. Origin and implications of troilite-orthopyroxene intergrowths in the brecciated diogenite Northwest Africa 7183. *Geochimica et Cosmochimica Acta* 220:125–145.

Zhang A. C., Kawasaki N., Bao H., Liu J., Qin L., Kuroda M., Gao J. F., Chen L. H., He Y., Sakamoto N., and Yurimoto H. 2020. Evidence of metasomatism in the interior of Vesta. *Nature Communications* 11.

SUPPORTING INFORMATION

Additional supporting information may be found in the online version of this article.

Table S1. EPMA analysis mean composition (wt%) of representative olivine, low-Ca pyroxene, and plagioclase in AM meteorites.

Zurfluh F. J., Hofmann B. A., Gnos E., Eggenberger U., and Jull A. J. T. 2016. Weathering of ordinary chondrites from Oman: Correlation of weathering parameters with C-14 terrestrial ages and a refined weathering scale. *Meteoritics & Planetary Science* 51:1685–1700.

Table S2. The EPMA analysis chemical composition (wt%) of the selected olivine and low-Ca pyroxene in the TPOI in AM 034.